Atmos. Chem. Phys. Discuss., 10, 2769–2808, 2010
www.atmos-chem-phys-discuss.net/10/2769/2010/

Atmospheric Chemistry and Physics Discussions

This discussion paper is/has been under review for the journal Atmospheric Chemistry and Physics (ACP). Please refer to the corresponding final paper in ACP if available.

Improvements in the profiles and distributions of nitric acid and nitrogen dioxide with the LIMS version 6 dataset

E. Remsberg[1], **M. Natarajan**[1], **T. Marshall**[2], **L. L. Gordley**[2], **R. E. Thompson**[2], **and G. Lingenfelser**[3]

[1]NASA Langley Research Center, 21 Langley Blvd., Mail Stop 401B, Hampton, VA 23681, USA
[2]GATS Incorporated, 11864 Canon Blvd., Suite 101, Newport News, VA 23606, USA
[3]SSAI, 1 Enterprise Parkway, Hampton, VA 23661, USA

Received: 14 December 2009 – Accepted: 22 January 2010 – Published: 3 February 2010

Correspondence to: E. Remsberg (ellis.e.remsberg@nasa.gov)

Published by Copernicus Publications on behalf of the European Geosciences Union.

Abstract

The quality of the Nimbus 7 Limb Infrared Monitor of the Stratosphere (LIMS) nitric acid (HNO_3) and nitrogen dioxide (NO_2) profiles and distributions of 1978/1979 is described after their processing with an updated, Version 6 (V6) algorithm and subsequent archival in 2002. Estimates of the precision and accuracy of both of those species are developed and provided herein. The character of the V6 HNO_3 profiles is relatively unchanged from that of the earlier LIMS Version 5 (V5) profiles, except in the upper stratosphere where the interfering effects of CO_2 are accounted for better with V6. The accuracy of the retrieved V6 NO_2 is also significantly better in the middle and upper stratosphere, due to improvements in its spectral line parameters and in the reduced biases for the accompanying V6 temperature and water vapor profiles. As a result of these important updates, there is better agreement with theoretical calculations for profiles of the HNO_3/NO_2 ratio, day-to-night NO_2 ratio, and with estimates of the production of NO_2 in the mesosphere and its descent to the upper stratosphere during polar night. The improved precisions and more frequent retrievals of the profiles along the LIMS orbit tracks provide for better continuity and detail in map analyses of these two species on pressure surfaces. It is judged that the chemical effects of the oxides of nitrogen on ozone can be examined quantitatively throughout the stratosphere with the LIMS V6 data, and that the findings will be more compatible with those obtained from measurements of the same species from subsequent satellite sensors.

1 Background

The Limb Infrared Monitor of the Stratosphere (LIMS) experiment was launched on 24 October 1978, on the near polar-orbiting Nimbus 7 satellite. LIMS operated from 25 October until 28 May 1979, measuring vertical radiance profiles across the atmospheric limb of the Earth (Gille and Russell, 1984). Its daily orbital data extend from

ACPD

10, 2769–2808, 2010

64° S to 84° N and are available at two local times per latitude (at about 1300 h and 2300 h at the Equator). The radiances were processed to infer middle atmospheric temperature profiles and the concentrations of several chemical compounds important for the chemistry of stratospheric ozone. LIMS provided profiles of ozone (O_3), water vapor (H_2O), nitric acid (HNO_3), and nitrogen dioxide (NO_2). Thus, LIMS was the first satellite experiment to provide a simultaneous, near-global view of the key chemical compounds in the ozone/nitrogen oxide photochemical chain. The temperature, geopotential height, and constituent profiles have been used for many scientific investigations, including effects of radiation on the net transport, responses of the middle atmosphere to perturbations, and correlations between the temperature and species data.

The LIMS Version 5 (or V5) profiles were archived in 1982; its measurements, algorithms, and data products are described in Gille and Russell (1984) and references therein. Since that time, significant improvements have been realized in the original spectroscopic parameters (Drayson et al., 1984) that were used for the V5 retrieval of temperature/pressure or *T(p)* and for the gaseous constituent profiles that contribute to the radiances measured within the six channels of LIMS. For this reason a reprocessing of the LIMS Level 2 (or profile) data to Version 6 (V6) was undertaken using the high-resolution, transmission molecular absorption line parameters of HITRAN 91/92 and/or 96. As a result, these V6 data are appropriate for comparisons with the temperature and species distributions obtained from the several middle atmosphere instruments onboard the NASA Upper Atmosphere Research Satellite (UARS), the Earth Observing System (EOS) Aura satellite and on the Canadian, European, and/or Japanese satellites SCISAT, ODIN, ENVISAT, and ADEOS.

A single LIMS scan profile began with the center of its FOV array viewing the horizon at 153 km altitude, moving downward to a point 38 km below the solid Earth limb and then returning upward. The angular resolutions (in milliradians) for the detectors of the FOV array are 1 mrad for the NO_2 and H_2O channels and 0.5 mrad for the other four channels, including HNO_3. The optical characteristics of all the channels are given in

Russell and Gille (1978, their Table 1). The V6 dataset was also improved by a better knowledge of the orbital attitude for the LIMS measurements, by using all the radiance profile samples, spaced 0.375 km in altitude, and by applying a multiple interleave retrieval process. Descriptions of the V6 algorithms for the conditioned radiances of all the channels and for the retrieval of the temperature and geopotential height profiles are in Remsberg et al. (2004). Characterizations of the improvements for V6 ozone and water vapor are provided in two additional papers (Remsberg et al., 2007 and 2009).

This paper is focused on the improvements and scientific implications for the V6 HNO_3 and NO_2 profiles and distributions. The V6 Level 2 data files contain both the de-convolved radiances and the retrieved parameters, and they are tabulated at 18 levels per decade of pressure or at a spacing of about 0.88 km. Note that the UARS Level 3A profiles have 6 levels of data per decade of pressure and represent a matching subset to the LIMS V6 data for easy comparison. In addition, the time, location, and solar zenith angle for the tangent point of a LIMS measurement are included in the header lines of each profile. This information makes it easier to relate the LIMS profiles of O_3, HNO_3, and NO_2 to photochemical model output. The effective vertical resolution for both V6 HNO_3 and NO_2 is of order 3.7 km, and retrievals were performed for each of the down/up scan pairs spaced about 1.6 degrees of latitude along the LIMS orbital tangent tracks. Distributions of HNO_3 extend from near the tropopause to just above the 2-hPa level. The nighttime distributions of NO_2 extend from about 50 hPa to the lower mesosphere, especially for the polar night. Results for daytime NO_2 are useful from about 50 hPa to 1 hPa.

Section 2 shows several daily, zonally-averaged distributions of the V6 HNO_3 and NO_2 for comparisons with model output and with distributions from more recent satellite experiments that also were observing during periods when the stratospheric aerosol loading was near background levels. An extensive validation of the V6 products was not conducted, although their daily zonal mean cross sections have been assessed against those of the V5 data that had been compared with the few correlative measurements available during the LIMS timeframe (e.g., Gille et al., 1984; Gille, 1987; Russell et al.,

ACPD
10, 2769–2808, 2010

1984a; Remsberg and Russell, 1987). Qualitative improvements have been found for all the V6 data products.

Section 3 describes the significant changes in the V6 algorithm that affect the V6 HNO_3 and NO_2 profiles. Independent estimates of precision and accuracy for those V6 data are included, based on calculations of the effects of their known error sources. The estimates of precision are shown to compare well with the variations in the retrieved parameters from among adjacent scans along an orbit, specifically for latitudes and times when zonal variations due to wave activity were minimal. Section 4 presents some scientific findings demonstrating the improved quality of the V6 HNO_3 and NO_2. Section 5 is a summary of our findings about the changes with V6.

2 Zonally-averaged distributions of HNO_3 and NO_2

Figure 1a and b are the zonally-averaged distributions of V6 HNO_3 from the combination of its Level 2 profiles along descending and ascending orbital segments for 15 November 1978, and 16 May 1979, respectively. Maximum mixing ratio values occur at the high latitudes near 30 hPa, and the variation of HNO_3 with latitude is similar to that from the earlier V5 dataset at that pressure level (Gille et al., 1984, 1993). However, the V6 HNO_3 profiles no longer exhibit nearly constant values in the upper stratosphere like those found from V5 by Jackman et al. (1985), due primarily to a better accounting for the effects of the interfering radiance from a "hot band" of carbon dioxide (CO_2) within the V6 algorithm. The V6 HNO_3 agrees reasonably well with photochemical model estimates; however, its day values are notably less than its night values near the 4-hPa level, most likely due to not having accounted for radiance contributions at higher altitudes from vibrationally-excited states of CO_2 and perhaps of O_3 in the 10 to 12-μm region during daylight (Edwards et al., 1996). V6 HNO_3 values are somewhat smaller than those of V5 in the lower tropical stratosphere, due to first-order corrections for the effects of interfering emissions from aerosols and from the chlorofluorocarbon (CFC) molecules $CFCl_3$ and CF_2Cl_2. The 1 ppbv contour extends to just above the

ACPD
10, 2769–2808, 2010

50-hPa level at equatorial latitudes; that value is at the upper limit of reactive nitrogen (NO_y) minus odd nitrogen (NO_x) from in situ measurements (Jensen and Drdla, 2002, and references therein).

One can see from Fig. 1a and b that there is very good seasonal symmetry between the HNO_3 distributions for November versus May of the Northern and Southern Hemispheres, which has already been explained by invoking heterogeneous chemical mechanisms (Austin et al., 1986). Note that there is an upward extension of moderately high values of HNO_3 to the upper stratosphere in November at high northern latitudes (Fig. 1a). This feature becomes prominent in winter due to a slow accumulation of HNO_3 after chemical conversion from NO_2 and dinitrogen pentoxide (N_2O_5) under polar night conditions. The distribution of 16 May (Fig. 1b) indicates that there was also an accumulation of HNO_3 in the 100 to 200-hPa layer in the Northern Hemisphere by late spring, due to diabatic descent in the region of the polar vortex.

Figure 2a and b show the zonally-averaged distributions of NO_2 from the descending (local nighttime at low and middle latitudes) and from the ascending (daytime at low and middle latitudes) orbital segments, respectively, for 15 November 1978. Maximum mixing ratio values for the nighttime LIMS NO_2 of Fig. 2a are of the order of 14 ppbv centered at about the 4-hPa level. The retrieved nighttime NO_2 profiles extend into the lower mesosphere, where they encounter their signal-to-noise (S/N) limit and are less accurate. The repartitioning of the NO_x (nitric oxide (NO)+NO_2) at twilight occurs at about 55 to 60° S latitude. Those terminator NO_2 profiles are also less accurate because the rapidly changing NO_2 values along the tangent path were not accounted for (see Solomon et al., 1986).

Maximum mixing ratios for the daytime NO_2 of Fig. 2b are of the order of 6 to 7 ppbv and occur between 8 and 10 hPa. One can clearly see the crossover to polar night conditions, poleward of about 72° N. Daytime NO_2 is small in the upper stratosphere because most of the NO_x is in the form of NO. H_2O emission becomes a significant part of the NO_2 channel radiance in the upper stratosphere, especially during daytime. The forward radiance model for the V6 NO_2 channel assumes that H_2O has a constant

value of 6.5 ppmv above the upper limit of 1.3 hPa for its V6 profile. Furthermore, there is a significant amount of extra emission in the mesosphere during daylight from excited states of the H_2O molecule that are difficult to characterize for LIMS, primarily because its ground-state H_2O populations are not known exactly in that region (Lopez-Puertas and Taylor, 2001; Kerridge and Remsberg, 1989). For this reason no corrections for non-LTE effects from H_2O were developed for the retrieval of the V6 NO_2. That source of positive radiance bias is the primary reason for the spurious, upward extension of the daytime NO_2 distributions to the lower mesosphere (see also Sects. 3 and 4).

Figure 3 is the distribution of NO_2 from the descending (nighttime) orbital segments of 15 January 1979, and it is similar to that of Fig. 2a in most respects. One exception is the occurrence of relatively large values of NO_2 near 50° S compared with those at equatorial latitudes. This difference is partly a diurnal effect. The LIMS NO_2 measurements were obtained at about 2130 h (local time) at 50° S versus 2300 h at the equator for the descending orbital segments, and there is a steady conversion of NO_2 to N_2O_5 from just after sunset and until sunrise. Furthermore, sunset occurs later in the day during summer at the high southern latitudes.

The elevated values of NO_2 in the mesosphere at the high latitudes of the Northern Hemisphere are another feature of Fig. 3. Such enhanced values of NO_2 were first reported by Russell et al. (1984b) based on a special, radiance-averaged version of the LIMS data, and they were attributed to the formation of NO_x in the mesosphere followed by a gradual descent of the air to the uppermost stratosphere during polar night. Findings from more recent satellite sensors support that conclusion (e.g., Randall et al., 2009). A time series of the V6 polar night NO_2 will be shown in Sect. 4, indicating improved estimates for its values and better continuity for its descent during the winter months of 1978/1979.

3 LIMS V6 retrieval algorithms and error estimates

3.1 The V6 algorithm for HNO_3 and NO_2

New emissivity data tables were prepared for the forward models of the primary gases in both the HNO_3 and NO_2 channels. The HNO_3 channel contains secondary radiance contributions from the "hot band" of CO_2 at 10.4 micrometers and from the primary CFCs ($CFCl_3$ and CF_2Cl_2). To achieve better accuracy for the emissivity of CO_2 along a tangent ray path, emissivity look-up tables were calculated at 55 pressure levels and 33 temperature levels and encompassing their expected atmospheric ranges. In addition, polynomial fits are no longer applied to account for the temperature dependence within the emissivity tables; linear interpolation is used instead. These upgrades have led to a more accurate representation of the effects of the "hot band" of CO_2.

The V6 forward model for the primary gas, HNO_3, makes use of emissivity tables generated using its band model data on HITRAN 91 (Rothman et al., 1992a). That model is based on the laboratory measurements of Giver et al. (1984), and a parameterization of them is appropriate for the broadband channel of LIMS. The interfering effects of CO_2 and of its "hot band" at 10.4 µm were obtained using the line parameters on HITRAN 92 (Rothman et al., 1992a and b; Dana et al., 1992), which are improved over the parameters used with the original LIMS V5 algorithm. To summarize, the updated emissivity tables for CO_2 account for much of the excess of retrieved HNO_3 that characterized the V5 HNO_3 profiles from about 5 to 2 hPa, as originally reported in Gille et al. (1984, 1993) and Jackman et al. (1985) (see also Sect. 4).

Line parameters for the original V5 retrievals of NO_2 were obtained from the AFGL trace gas compilation (Rothman et al., 1981). Spin-rotation effects of NO_2 became known by the late 1980s, and the fine structure of the lines for the primary ν_3 cold band were included in the HITRAN 92 compilation via a perturbation calculation (Perrin et al., 1992). That change accounts for most of the improvements in the V6 NO_2 (Remsberg et al., 1994). Further, minor changes in the retrieved NO_2 may be found for those spin-rotation effects from the more explicit calculations of the strengths of the

ACPD
10, 2769–2808, 2010

resolved lines that were obtained later and are available in HITRAN 96 (Toth, 1992). The LIMS NO_2 channel also contains contributions from H_2O, CH_4, and the oxygen (O_2) continuum. Spectral parameters for the underlying O_2 were not available, so the empirical model of Thibault et al. (1997) was used for consistent calculations of the effects of the continuum-induced absorption from O_2 in both the H_2O and the NO_2 channels.

The LIMS V6 profiles were used to correct for the forward radiance contributions of H_2O up to about the 1.5-hPa level, and then they were extended upward using a constant value of 6.5 ppmv. In addition, the entire H_2O profile for the forward model was smoothed by a Gaussian function having a 1.5 km half-width at half maximum. As indicated earlier, no corrections were developed to account for probable non-LTE radiances from mesospheric H_2O during daytime. Even so, there is no indication of a bias in the retrieved NO_2 due to that neglect, except at and above about 48 km (or the 1-hPa level). Emissions from excited states of daytime NO_2 were postulated for the upper stratosphere by Kerridge and Remsberg (1989), but no correction for those effects was developed for V6 because the populations of those states are not known well. The effects of horizontal mixing ratio gradients in the tangent layer have also been shown to be important for the retrieval of LIMS NO_2 in the region of the day/night terminator (Solomon et al., 1986). However, because such a gradient correction is needed only for solar zenith angles near 90 degrees, a second-pass processing was not considered for the V6 NO_2 profiles prior to their archival in 2002.

The original V5 profiles of NO_2 and HNO_3 are used as a priori estimates for the V6 forward models, although there is no dependence upon them for the onion-peeling retrievals of LIMS once a reasonable S/N for the radiances is achieved. Estimated concentrations of the interfering gases were obtained as follows. Updated, seasonal zonal-mean distributions of CH_4 were generated from the UARS HALOE dataset for use with the V6 retrievals of NO_2 but with an extrapolation of their magnitudes back to 1979, based on the approximate linear emission rate for CH_4 at the ground. A similar extrapolation was performed for $CFCl_3$ and CF_2Cl_2 for the HNO_3 channel, based on

their measured distributions from the UARS CLAES Version 8 dataset plus knowledge of the growth rates for their emissions since 1975.

Interfering emission due to aerosols has its largest effect on the LIMS-retrieved HNO_3 at low latitudes of the lower stratosphere; the LIMS V5 dataset had no such correction. A first-order broadband emission was generated for V6, based on estimates for the background stratospheric aerosol layer of 1978/1979. Specifically, a single zonal-mean distribution of aerosol extinction was adopted for the V6 algorithm based on March/May 1996 results for the HALOE 5.26 µm (NO) channel (Hervig et al., 1995). The magnitude of that distribution was then scaled back to 1978/1979 using a factor obtained by comparing the SAGE II 1-µm channel aerosol extinction values of 1996 versus the SAGE I aerosol extinction for the same months of 1979. That single modified, zonal mean aerosol distribution was used for each of the seven months of the LIMS dataset and must be considered as somewhat qualitative with latitude and likely not representative of its seasonal cycle variations. However, tropical aerosol distributions vary most noticeably according to the phase of the QBO cycle, and both the 1996 and 1979 March/May periods occurred at nearly the same QBO phase. Finally, aerosol extinction at the wavelengths of the LIMS channels versus that at 5.26 µm of HALOE was obtained by employing the sulfuric acid/H_2O composition and wavelength-dependent, refractive index model for its aerosol absorption in the manner of Hervig et al. (1995).

The archived V6 profiles were screened for anomalies using several criteria. First, retrieval variances were calculated and written to an intermediate Level 2 file that was not archived. Those variances were defined in terms of $(NEN/K)^2$, where NEN is the noise equivalent radiance for each channel in watts/m^2-sr (Gille and Russell, 1984) and K is the derivative of the measured signal profile as a function of the given species mixing ratio. During the retrieval process the variances were set to the negative of their actual values whenever convergence was not achieved or the retrieval needed to be restarted (at tops of profiles). Note that a restart causes the algorithm to default to a constant, top-layer, mixing ratio based on the value from the layer of its first,

successfully-retrieved level; the thickness of that constant, top-layer extends upward several scale heights. Valid profile segments have positive variances, and only retrieved values from those segments were retained in the final Level 2 output file. The variance parameters effectively set the extreme upper altitude limits for good data for all the parameters. Negative variances often indicate the low altitude extent of good data, too. Variance checking occurred only outside of the pressure ranges of 1.9 hPa to 46 hPa for HNO_3 and of 0.88 hPa to 46 hPa for NO_2. Independent estimates of random error indicate that there is adequate tangent layer signal within those ranges. An additional algorithm was applied to identify and screen for contaminating radiances from cloud tops, at least to first order (see Remsberg et al., 2007, for the details).

3.2 Single profile error estimates

The V6 HNO_3 profile values are not much different from those of V5, except in the upper stratosphere where the interference from CO_2 has been accounted for better in the V6 algorithm. In the lower tropical stratosphere there are differences due to the corrections for emissions from the CFCs and due to the first-order correction for the aerosol emission. Random radiometric errors for V6 HNO_3 are reduced from those of V5 by a factor of 2.2 because of the larger number of samples used with the interleave procedure for the retrieval of a V6 profile (Remsberg et al., 2004). Offset errors due to pointing jitter are included in the random uncertainties. The calculated precisions shown in Fig. 4 vary from 0.15 ppbv at 80 hPa to 0.05 ppbv at 3 hPa, based on the average profile at 30° S. Those calculated values are provided in percent in the top row of Table 1, and they compare well with empirical estimates of the precision from the Level 2 data themselves – the standard deviation (SD) profile in Fig. 4. The SD values were obtained as minima of the variances for each pressure level from among the sets of scans along each of the orbits that crossed 25° S to 35° S latitude on 1 February 1979. Of course, a part of the empirical SD values in Fig. 4 may be a result of real variations in the atmospheric HNO_3.

Sources of systematic uncertainty were reported in Gille et al. (1984), based on simulations of their effects for V5 from a model HNO_3 profile for 32° N. Many of those error estimates are retained for V6, as shown in the middle rows of Table 1. However, the effects of temperature bias are based on the revised estimates of *T(p)* error in Remsberg et al. (2004). Uncertainties in the aerosol and CFC corrections are greatest for the lower tropical stratosphere but do not dominate the total error during 1978/1979. Biases at the tops of the V6 HNO_3 profiles are small because the a priori profile values are also small near the stratopause and extend above the pressure level of the first retrieved point. Uncertainties for the effects of the horizontal temperature gradients are not included, since sensitivity to temperature biases are relatively small for an optically thin species like HNO_3.

The largest elements of potential bias error are the ±20% uncertainties in the integrated areas of the field-of-view (FOV) side lobes and from a possible 0.05% bias in the total measured signal due to regions of the channel filter that are outside the main spectral band, as discussed in Gille et al. (1984) and shown in the bottom rows of Table 1. The FOV side lobes from the HNO_3 channel are not all of the same sign. To judge their effects, the measured HNO_3 radiance profiles were analyzed for the vertical distances of the side lobes from the main HNO_3 lobe or at effective separations of 17 and 34 km at the horizon. For instance, are there any positive or negative radiance correlations at those separations when the main lobe is viewing the low radiances of the mid to upper stratosphere and when the side lobes are viewing the much larger radiances at altitudes 17 or 34 km below? Our investigations indicate no significant correlations for altitudes below about 40 km. Thus, it is concluded that the magnitude of that error in Table 1 must be an upper limit at all levels, except perhaps at 3 hPa. Uncertainties for the out-of-band spectral response can impart a positive bias in HNO_3 of order 20% at 30 hPa, as pointed out in Gille et al. (1984). Yet, qualitative comparisons with other HNO_3 datasets indicate agreement that is better than 20%, at least for those datasets that were obtained at times of relatively low stratospheric aerosol loading. Therefore, neither of those sources of error is included in the combined root-sum-squares (RSS)

estimates of accuracy in Table 1. In summary, the overall accuracy for V6 HNO_3 is believed to be very good from 30 hPa to 10 hPa – of order 10% at middle latitudes.

Table 2 contains the estimates of precision and accuracy for the profiles of NO_2. First, the reader is reminded that the nighttime values of V6 NO_2 have peak mixing ratios near 4 hPa that are about 15% to 20% lower than those of V5. Most of that change is due to the effects of the spectral spin splitting of the strong lines that was not included in earlier versions of the AFGL or HITRAN line lists. On the other hand, the peak daytime V6 NO_2 values at 8 to 10 hPa are reduced from V5 by only about 5% because the effect of saturation for the strongest lines is not nearly so pronounced for the lower mixing ratios of daytime. In the upper stratosphere near 3 hPa, the daytime V6 NO_2 is larger than that of V5 due to the improved values from the interfering V6 H_2O. Below the 30-hPa level of the lower stratosphere both the day and night V6 NO_2 values are somewhat larger than V5. At this point it is noted that the V5 algorithm contained a merger of its retrieved NO_2 with a balloon-based average NO_2 profile from 30° N, constraining its results below the 30-hPa level at least when the S/N for the tangent-layer radiance was low. The V6 NO_2 algorithm is not constrained by any such climatological profile.

The precision estimates for the V6 NO_2 in Table 2 were adopted from those of V5 in Russell et al. (1984a), after accounting for the improvements due to the use of all the samples from the measured radiance profiles. Random uncertainties from single profiles of the retrieved H_2O were adopted from Remsberg et al. (2009) and included because H_2O is a major source of interfering emission, especially for daytime NO_2 in the upper and the lowermost stratosphere. The effects of those random H_2O errors are scaled further, according to the fraction of the signal in the NO_2 channel that is due to H_2O. Estimates of percentage NO_2 precision profiles from the data are shown in Fig. 5 and are based on average day and average nighttime SD profiles at 30° S for 1 February 1979. Those values range from about 5% in the middle stratosphere, to 8% for nighttime or 30% for daytime at 1 hPa, and then to 15–20% at 40 hPa. The estimated SD values in Fig. 5 agree with the RSS precisions in Table 2 for the middle and upper stratosphere but are larger at 30 and 50 hPa, presumably because of the

ACPD
10, 2769–2808, 2010

effects of the natural variability of the atmospheric NO_2.

For the V6 NO_2 bias errors a linear scaling was applied to the entries in the V5 error table of Russell et al. (1984a), which were appropriate for a model-generated, daytime profile at 32° N. Its primary sources of systematic uncertainty are from temperature bias and from the interfering effects of H_2O, based on the V6 uncertainties in Remsberg et al. (2004, 2009), respectively. There are uncertainties in the lower stratosphere due to the O_2 interference, but they should be considered as an upper limit because corrections for its emission were applied to the retrievals of both the LIMS H_2O and NO_2 and therefore carry the same sign. There is also a possible bias due to a 20% uncertainty for the area of the measured FOV side lobes, but its effect on the retrieved NO_2 is small and remains unverified.

Table 2 indicates RSS V6 NO_2 uncertainties of 17% at 3 hPa and about 18% from 5 to 10 hPa. RSS values increase sharply in the lower stratosphere and are dominated by the estimates of error for the interfering O_2 continuum and the H_2O. At stratopause levels (1 hPa) the ascending (daytime) NO_2 may have a bias of order 33% across most latitudes. However, the larger, descending (nighttime) NO_2 values at that level are not affected much by the interfering H_2O, so they are more accurate (17%). Also, the increasing values of NO_2 in the lower mesosphere at the high northern latitudes of Fig. 3 are judged to be reasonably accurate (see also Sect. 4.4). One source of bias error that has been neglected for that situation is the likelihood that the retrieved V6 polar night NO_2 values are too low due to not accounting for the effects of non-LTE emissions of the ground-state of NO_2 itself (e.g., see Funke et al., 2005).

4 Scientific implications of the V6 data

The previously, archived LIMS V5 HNO_3 and NO_2, along with the temperature, O_3, and H_2O data have been used in scientific studies and reported in the literature. In the subsections that follow several of the issues that they raised with respect to the

ACPD
10, 2769–2808, 2010

V5 HNO_3 and NO_2 profiles and distributions are re-visited and re-evaluated using the V6 data.

4.1 HNO_3/NO_2 ratio profiles

Simultaneous measurements of HNO_3 and NO_2 by LIMS provide an opportunity to check the partitioning of NO_y species in comparison with that predicted with theoretical models. In particular, Jackman et al. (1985) reported that between 5 and 1 hPa the ratio of LIMS daytime HNO_3 to NO_2 was inconsistent with model values and that the HNO_3 derived from photochemical relations should be used instead of those from the LIMS. They based their conclusion on a comparison of daytime hydroxyl (OH) values derived from the V5 data using two different procedures. In the first approach they invoked an instantaneous photochemical equilibrium assumption for HNO_3 and, thereby, expressed OH concentrations as a function of the ratios of HNO_3/NO_2. Their second approach used an equilibrium assumption for odd hydrogen (HO_x) along with the LIMS O_3 and H_2O data to derive the daytime OH values. In the upper stratosphere those two approaches yielded different results. The V5 HNO_3/NO_2 ratios overestimated OH in the upper stratosphere by a large margin, at least when compared to other available observations and model results. The second approach yielded much better agreement. Jackman et al. (1985) concluded that this discrepancy was due to errors in the LIMS HNO_3 in the 5 to 1 hPa region. Natarajan et al. (1986) reached a similar conclusion regarding the HNO_3/NO_2 ratio, but on the basis of diurnal photochemical model calculations that were constrained by LIMS V5 nighttime data. The V5 HNO_3/NO_2 ratios also showed a positive bias in the upper stratosphere in comparison with their modeled estimates.

Figure 6 is a comparison of the daytime ratio of V6 HNO_3/NO_2 for 15 February 1979, versus that from the updated, diurnal photochemical model of Natarajan et al. (2002), which incorporates the recommended chemical kinetics data of Sander et al. (2006). Distributions of long-lived species, such as nitrous oxide (N_2O), that are used to initialize the diurnal calculations are taken from a simulation with the NASA Langley

two-dimensional model of Callis et al. (2001) using surface source gas mixing ratios corresponding to the 1978/1979 time period. The bottom panel of Fig. 6 shows LIMS HNO_3/NO_2 ratios that are less than 0.2 in the upper stratosphere, except at the winter high latitudes. At the top boundary of the data domain (near 2 hPa) the V6 ratios are lower than the ones from the V5 data. The better determination of the V6 temperature profile and its effects for the "hot band" of CO_2 has led to a large decrease in the retrieved, upper stratospheric HNO_3 and a corresponding decrease in the HNO_3/NO_2 ratio. The model results are shown in the top panel, and they agree well with the ratios from the V6 data.

The HNO_3/NO_2 ratios in Fig. 6 from both the model and LIMS show a steady decline with decreasing pressure, although the LIMS ratios are larger at the top-most boundary. The reason for that remaining disagreement is most likely a high bias in the daytime HNO_3 due to the influence of non-LTE emission in this spectrally-broad channel that has not been corrected. Edwards et al. (1996) also observed differences between the day and night radiances of the 10.83-µm blocker channel of the Cryogenic Limb Array Etalon Spectrometer (CLAES) instrument, and they ascribed them to non-LTE effects from ozone and CO_2 near the stratopause during daytime. Estimations of the effects of those emissions on the retrieved HNO_3 were not obtained for this paper. However, it is noted that the lifetime of HNO_3 against photolysis in the upper stratosphere is several hours and, therefore, an assumption of instantaneous equilibrium between HNO_3 and NO_2 is not strictly valid at the local measurement times of LIMS across all latitudes. Such an assumption introduces uncertainties in both the evaluation of the OH concentration from the ratio HNO_3/NO_2 and in the derivation of HNO_3 based on OH values from other sources. Nevertheless, because of the improved results from LIMS V6 there is no need to substitute model daytime HNO_3 for the retrieved LIMS values in the upper stratosphere.

4.2 Lower stratospheric HNO_3 and NO_y

The LIMS dataset provides global scale information on the latitudinal distribution of stratospheric HNO_3 and NO_2. Earlier analyses of the V5 data in conjunction with model studies highlighted a deficiency with respect to the HNO_3 mixing ratios of the winter high latitudes as calculated by models using only gas-phase chemistry. For instance, Austin et al. (1986) compared LIMS V5 HNO_3 with other measurements and model results. They reported that an additional source of HNO_3 was needed at high latitudes in winter and suggested that the hydrolysis of N_2O_5 on aerosol surfaces could be important. Considine et al. (1992) also described results from their two-dimensional model compared with the V5 data and noted the importance of heterogeneous chemistry for their calculations of HNO_3. They also pointed out that while the inclusion of heterogeneous chemistry improved the model/data agreement for HNO_3, its addition led to larger discrepancies between the calculated and observed NO_2.

At this point it is emphasized that the latitudinal variations of the lower stratospheric HNO_3 and NO_2 from the V6 algorithm are very similar to those from V5 and also similar to the observations from several more recent satellite instruments (not shown). This lack of change is not surprising because the updated spectroscopic line parameters for V6 have very little effect on their retrieved lower stratospheric mixing ratios. However, minor changes from V5 to V6 were noticed at tropical latitudes due to the improved treatments for the interfering species.

The dashed curve in the top panel of Fig. 7 shows zonally-averaged V6 HNO_3 at 30 hPa as a function of latitude for December 1978. The solid line corresponds to the HNO_3 from the two-dimensional model of Callis et al. (2001), which includes a formulation for heterogeneous chemistry similar to contemporary models. The model HNO_3 agrees with the data reasonably well with respect to their latitudinal distributions, showing higher mixing ratios at winter high latitudes. The vertical line represents the estimated LIMS uncertainty of 8% (Table 1) based on a mid-latitude summer profile. It is clear that the LIMS HNO_3 is higher than that of the model and has a different slope

across the middle latitudes, particularly for the winter hemisphere. Figure 8 shows the V6 HNO_3 distribution on the 31.6 hPa surface for early January 1979, and it exhibits a lot of zonal variability at middle and high latitudes of the Northern Hemisphere. Remsberg and Bhatt (1996) showed that the effects of wave activity led to the pattern of the middle latitude surf zone plus a subtropical barrier region by early January. It is difficult to simulate such a pattern with the parameterized transport of a two-dimensional model. Conversely, there is little to no zonal variability in Fig. 8 for the tropics, where the LIMS and model results agree well in Fig. 7.

The lower panel of Fig. 7 shows the latitudinal variations of the sum of LIMS V6 descending or nighttime HNO_3 and NO_2 mixing ratios (dashed line) versus the model calculated total NO_y (solid line). The nighttime LIMS (HNO_3+NO_2) data should be considered as a lower bound for the total NO_y because the contribution from other nitrogen containing species, such as N_2O_5 and $ClONO_2$, is likely non-negligible. Again, the vertical line is the uncertainty for the data obtained as the RSS of the estimated errors of NO_2 and HNO_3. The model estimate of the total NO_y is clearly lower than that inferred from LIMS. It is recognized though that the level of agreement between the data and model comparisons of Fig. 7 depends on the sources of NO_y, such as N_2O, and to the transport formulations used in the model. For a given NO_y distribution the effect of heterogeneous chemistry increases the ratio of HNO_3/NO_2 in the model.

Figure 9 is a polar plot of the Northern Hemisphere distribution of LIMS V6 nighttime NO_2 at 31.6 hPa for 5 January 1979. Note that the distribution shows a decrease from about 3 ppbv in the tropics to less than 1.8 ppbv poleward of about 40° N, a clear indication of the so-called "Noxon cliff phenomenon" (Noxon, 1979). This wintertime decrease of NO_2 with latitude was not so apparent and coherent within the V5 dataset. One can now readily follow the evolution of this feature with the V6 data. It is an example of another improvement that has been gained for NO_2 with the V6 algorithm.

ACPD
10, 2769–2808, 2010

4.3 Day-to-night NO_2 ratios

The availability of day and nighttime measurements of a diurnally varying species like NO_2 allows one to examine the photochemistry of this species using theoretical models in conjunction with data. For example, Solomon et al. (1986) used LIMS nighttime NO_2 data at high northern latitudes in May to show that the decay of NO_2 to form N_2O_5 was consistent with theory. On the other hand, Kerridge and Remsberg (1989) examined profiles of the day-to-night ratios of NO_2 and found a region of discrepancy with theory in the upper stratosphere. In particular, the LIMS V5 data showed much larger ratios than expected from photochemical models above about 42 km (or 2 hPa).

An updated comparison of the day-to-night NO_2 ratio profiles from the V6 data is shown in Fig. 10 along with those from a contemporary, diurnal photochemical model. Monthly average LIMS results for May 1979 are in the bottom panel, and they show steadily declining ratios at levels above 5 hPa, reaching a minimum of less than 0.05 at 1.0 hPa before increasing to about 0.15 at 0.5 hPa. The photochemical model simulations were conducted using results from the two-dimensional model of Callis et al. (2001) for initialization. The model day-to-night NO_2 ratios are shown in the top panel and correspond to the local times of the LIMS day and night measurements. The model ratios are in good agreement with the data in the 5 to 1 hPa region but continue to show decreasing values in the lower mesosphere. Interfering radiance from H_2O is the primary source of uncertainty for the LIMS forward model of NO_2 at upper altitudes, especially for daytime. H_2O was accounted for by considering the retrieved H_2O up to 1.5 hPa plus a fixed H_2O value above that level, even though non-LTE emissions from H_2O are known to be significant in the lower mesosphere (Remsberg et al., 2009). As with V5, the LIMS V6 algorithm does not correct for such non-LTE effects, leading to a positive bias in the retrieved daytime NO_2. In addition, Kerridge and Remsberg (1989) postulated a possible role for non-LTE emissions during daytime from NO_2 itself. But in a recent analysis of the spectrally-resolved NO_2 measurements from the MIPAS instrument of ENVISAT, Funke et al. (2005) found no evidence for non-LTE emissions

from higher-vibrational states of NO_2, at least for altitudes below 50 km. Therefore, it is concluded that any non-LTE effects from NO_2 must be secondary to the much larger influence of the non-LTE emissions from H_2O. It is estimated that the upper boundary region of accurate V6 daytime NO_2 values is 1.5 to 1.0 hPa.

4.4 Mesospheric NO_2 during polar night

The production of NO_x in the mesosphere and lower thermosphere by energetic particle precipitation has been described in connection with its downward transport into the high latitude winter stratosphere (e.g., Callis et al., 2001; Natarajan et al., 2004; Randall et al., 2006). Russell et al. (1984b) reported the first satellite-based observation of wintertime increases in upper stratospheric NO_2. Upon averaging 5 days of LIMS radiances within a 60-degree longitude sector, they were able to extend their retrievals of LIMS NO_2 to higher altitudes. By focusing on polar night conditions in January 1979, they obtained NO_2 mixing ratios exceeding 100 ppbv in the lower mesosphere. Although odd nitrogen can be produced directly by solar proton events in the high latitude upper stratosphere, there is no evidence of such high-energy events in January 1979. The enhanced NO_2 in the LIMS data must be due to transport processes following the production of NO_x by energetic particle precipitation in the mesosphere and above, the so-called "indirect effect" (Randall et al., 2006).

The V6 algorithm does not employ a radiance-averaging procedure, so the single profiles of V6 NO_2 extend only up to about 0.15 hPa at the winter high latitudes. Elevated mixing ratios of NO_2 are still found in the mesosphere (Fig. 3), although those values are lower than reported in Russell et al. (1984). Nevertheless, these V6 values are considerably higher than what is expected if there are only stratospheric sources of NO_x. The occurrence of smaller V6 NO_2 mixing ratios is primarily because the V6 radiance profiles are registered better and the V6 temperatures are warmer by as much as 6 K at 0.1 hPa (Remsberg et al., 2004). Although the single profile error estimates for NO_2 in Table 2 apply strictly to its climatological profile and do not extend to altitudes above 1 hPa, the effects of a 2 K temperature bias and of an H_2O bias at 1 hPa are 10%

and 28%, respectively. Total error in Table 2 for NO_2 is estimated to be 33% at 1 hPa. The EOS Aura MLS experiment is obtaining H_2O that has relatively small values in the wintertime, polar vortex regions of the mesosphere (http://mls.jpl.nasa.gov/). Thus, the uncertainties due to the interfering effects of H_2O on the V6 NO_2 are estimated to be reduced considerably in that situation.

Figure 11 is a time series of the zonally-averaged V6 nighttime NO_2 mixing ratio as a function of pressure for latitudes greater than 74° N. Data from 1 November 1978 to 31 March 1979 are represented. For the several days when the LIMS instrument did not take data, their NO_2 values are averages from the adjacent days at all pressure levels. NO_2 mixing ratios exceeding 10 ppbv occurred in the 0.2 to 0.5 hPa region from late November 1978 to early February 1979 along with a clear indication of atmospheric descent with time of that elevated NO_2. Comparisons of the fields of geopotential height and nighttime NO_2 during January at 0.46 hPa indicate that the highest NO_2 values corresponded to observations within the polar vortex region (not shown). The reaction of NO_x with O_3 in the upper stratosphere leads to a gradual conversion of NO_2 to nitrogen trioxide (NO_3) and then to N_2O_5 in the polar night region. The NO_2 variation in Fig. 11 between 2 and 10 hPa and during November and December is mostly a result of transport of air from lower latitudes followed by a photochemical conversion of its NO_2. In particular, early December 1978 was the time of a wave-1 stratospheric (Canadian) warming event. The LIMS observations of Fig. 11 provide support for the hypothesis that under such dynamic conditions there can be increases of high latitude upper stratospheric NO_x as a result of accelerated descent within the polar vortex. More dramatic perturbations, such as solar proton events, are not a necessary condition for such enhancements of upper stratospheric NO_x.

5 Summary findings

The radiances of the Nimbus 7 LIMS experiment have been reconditioned and new retrievals of them conducted with an updated (V6) algorithm to generate HNO_3 and

ACPD
10, 2769–2808, 2010

NO_2 profiles that are more compatible with those of follow-on satellite experiments. The V6 HNO_3 profiles are nearly unchanged in the middle and lower stratosphere from those of the earlier V5 algorithm. However, in the upper stratosphere V6 HNO_3 is smaller due to improvements in the accounting for interfering emissions from CO_2. That change yields daytime HNO_3/NO_2 ratios that agree better with results from theoretical model calculations than before. The V6 NO_2 profiles have smaller values than those of V5, most noticeably for nighttime profiles of the upper stratosphere due to the accounting of spin-rotation effects within the updated, spectroscopic line parameters of NO_2. More accurate retrievals of the V6 temperature and H_2O from the lower mesosphere to near the stratopause are responsible for the realistic V6 NO_2 profiles of that region of the atmosphere, most notably in the polar night regions. Day-to-night ratios of V6 NO_2 also agree well with photochemical model calculations in the middle and upper stratosphere.

Individual V6 profiles of HNO_3 and NO_2 have points every 0.375 km and an effective vertical resolution of 3.7 km. The V6 retrievals were applied to adjacent pairs of profiles along orbits, yielding a spacing of 1.6 degrees of latitude between retrieved profiles, on average. Single HNO_3 profiles have precisions of 3–4% from 10 to 50 hPa but of order 10% at 3 hPa and 21% at 80 hPa. Single NO_2 profiles have precisions of 4–6% from 3 to 10 hPa, 6% at 30 to 50 hPa, and 14% at 1 hPa. The improved precisions and more frequent retrievals of profiles along the orbit tracks provide better continuity and detail for mapping analyses of these two species on pressure surfaces.

Estimated accuracies for single profiles of V6 HNO_3 are better than 10% from 10 to 50 hPa, and about 12% at 3 hPa and 16% at 80 hPa. Estimates of accuracy for the V6 NO_2 profiles are of order 18% from 3 to 10 hPa, but degrading to about 30% at 30 hPa and 1 hPa. Even so, good quality retrievals of V6 NO_2 extend downward to at least the 50-hPa level at polar latitudes in northern winter, which was not the case for NO_2 from the earlier V5 dataset. A time series plot of V6 NO_2 at northern high latitudes illustrates NO_x enhancement through wintertime descent from the lower mesosphere to the upper stratosphere. This finding is significant, especially when one considers that

ACPD
10, 2769–2808, 2010

there were no notable increases in solar disturbance or geomagnetic storm activity late in 1978 or early in 1979.

The V6 HNO_3 distributions suggest that one must still include heterogeneous chemical mechanisms in stratospheric models for the partitioning of NO_y, even during the 1978/1979 period of low volcanic aerosol loading. However, it is more apparent from the V6 data that there are deficiencies for the seasonal transport of the N_2O source molecule and of its end product NOy, as simulated with most two-dimensional models of the lower stratosphere.

The V6 Level 2 (profile) data can be obtained by ftp download from the Goddard Earth Sciences and Data Information Services Center or GES DISC (http://daac.gsfc.nasa.gov/) under the menu entitled "Remote Sensing Data." A LIMS V6 Level 3 (zonal Fourier coefficient or mapped) product is also available at GES DISC.

Acknowledgements. We recognize the extensive efforts of John Gille and Jim Russell III (Co-PIs) and the members of the original Project and Science Teams for their development and conduct of the LIMS experiment. Yun-fei Wang conducted analyses of the LIMS HNO_3 radiances for evidence of any spurious effects from its FOV side lobes. The research leading to the improvement and generation of the LIMS V6 Level 2 dataset was conducted with the consistent support of Jack Kaye of NASA Headquarters. The analyses in this manuscript were conducted with funds from the NASA NRA NNH08ZDA001N for the MAP Program administered by David Considine.

References

Austin, J., Garcia, R. R., Russell III, J. M., Solomon, S., and Tuck, A. F.: On the atmospheric photochemistry of nitric acid, J. Geophys. Res., 91, 5447–5485, 1986.

Butchart, N. and Remsberg, E. E.: The area of the stratospheric polar vortex as a diagnostic for tracer transport on an isentropic surface, J. Atmos. Sci., 43, 1319–1339, 1986.

Callis, L. B., Natarajan, M., and Lambeth, J. D.: Solar-atmospheric coupling by electrons (SOLACE), 3. Comparisons of simulations and observations, 1979–1997, issues and implications, J. Geophys. Res., 106, 7523–7539, 2001.

Considine, D. B., Douglass, A. R., and Stolarski, R. S.: Heterogeneous conversion of N_2O_5 to HNO_3 on background stratospheric aerosols: comparisons of model results with data, Geophys. Res. Lett., 19, 397–400, 1992.

Dana, V., Mandin, J.-Y., Guelachvili, G., Kou, Q., Morillon-Chapey, M., Wattson, R. B., and Rothman, L. S.: Intensities and self-broadening coefficients of $^{12}C^{16}O_2$ lines in the laser band region, J. Mol. Spectrosc., 152, 328–341, 1992.

Drayson, S. R., Bailey, P. L., Fischer, H., Gille, J. C., Girard, A., Gordley, L. L., Harries, J. E., Planet, W. G., Remsberg, E. E., and Russell III, J. M.: Spectroscopy and transmittances for the LIMS experiment, J. Geophys. Res., 89, 5141–5146, 1984.

Edwards, D. P., Kumer, J. B., Lopez-Puertas, M., Mlynczak, M. G., Gopalan, A., Gille, J. C., and Roche, A.: Non-local thermodynamic equilibrium limb radiance near 10 µm as measured by UARS CLAES, J. Geophys. Res., 101, 26577–26588, 1996.

Funke, B., Lopez-Puertas, M., von Clarmann, T., Stiller, G. P., Fischer, H., Glatthor, N., Grabowski, U., Hoepfner, M., Kellmann, S., Kiefer, M., Linden, A., Mengistu Tsidu, G., Milz, M., Steck, T., and Wang, D.-Y.: Retrieval of stratospheric NO_x from 5.3 and 6.2 µm nonlocal thermodynamic equilibrium emissions measured by Michelson Interferometer for Passive Atmospheric Sounding (MIPAS) on Envisat, J. Geophys. Res., 110, D09302, doi:10.1029/2004JD005225, 2005.

Gille, J. C.: Distributions of ozone and nitric acid measured by the limb infrared monitor of the stratosphere (LIMS), in: Transport Processes in the Middle Atmosphere, edited by: Visconti, G. and Garcia, R., D. Reidel Publ. Co., Dordrecht, Holland, 73–85, 1987.

Gille, J. C. and Russell III, J. M.: The limb infrared monitor of the stratosphere: experiment description, performance, and results, J. Geophys. Res., 89, 5125–5140, 1984.

Gille, J. C., Bailey, P. L., and Craig, C. A.: Revised reference model for nitric acid, Adv. Space Res., 13, 59–72, 1993.

Gille, J. C., Russell III, J. M., Bailey, P. L., Remsberg, E. E., Gordley, L. L., Evans, W. F. J., Fischer, H., Gandrud, B. W., Girard, A., Harries, J. E., and Beck, S. A.: Accuracy and precision of the nitric acid concentrations determined by the limb infrared monitor of the stratosphere experiment on NIMBUS 7, J. Geophys. Res., 89, 5179–5190, 1984.

Giver, L. P., Valero, P. J., and Goorvitch, D.: Nitric acid band intensities and band-model parameters from 620 to 1760 cm^{-1}, J. Opt. Soc. Am. B, 1, 715–722, 1984.

Hervig, M. E., Russell III, J. M., Gordley, L. L., Daniels, J., Drayson, S. R., and Park, J. H.: Aerosol effects and corrections in the Halogen Occultation Experiment, J. Geophys. Res., 100, 1067–1079, 1995.

Jackman, C. H., Kaye, J. A., and Guthrie, P. D.: LIMS HNO_3 data above 5 mbar: corrections based on simultaneous observations of other species, J. Geophys. Res., 90, 7923–7930, 1985.

Jensen, E. and Drdla, K.: Nitric acid concentrations near the tropical tropopause: implications for the properties of tropical nitric acid trihydrate clouds, Geophys. Res. Lett., 29(2001), 62-1–62-4, doi:10.1029/2002GL015190, 2002.

Kerridge, B. J. and Remsberg, E. E.: Evidence from the limb infrared monitor of the stratosphere for nonlocal thermodynamic equilibrium in the ν_2 mode of mesospheric water vapour and the ν_3 mode of stratospheric nitrogen dioxide, J. Geophys. Res., 94, 16323–16342, 1989.

Lopez-Puertas, M. and Taylor, F. W.: Non-LTE radiative transfer in the atmosphere, World Scientific Publishing Co. Pte. Ltd., London, 487 pp., 2001.

Natarajan, M., Callis, L. B., Boughner, R. E., Russell III, J. M., and Lambeth, J. D.: Stratospheric photochemical studies using Nimbus 7 data, 1. Ozone photochemistry, J. Geophys. Res., 91, 1153–1166, 1986.

Natarajan, M., Remsberg, E. E., and Gordley, L. L.: Ozone budget in the upper stratosphere: Model studies using the reprocessed LIMS and the HALOE datasets, Geophys. Res. Lett., 29, 1152, 56-1–56-4, 2002.

Natarajan, M., Remsberg, E. E., Deaver, L. E., and Russell III, J. M.: Anomalously high levels of NO_x in the polar upper stratosphere during April, 2004; Photochemical consistency of HALOE observations, Geophys. Res. Lett., 31, L15113, doi:10.1029/2004GL020566, 2004.

Noxon, J. F.: Stratospheric NO_2, 2. Global behavior, J. Geophys. Res., 84, 5067–5076, 1979.

Perrin, A., Camy-Peyret, C., and Flaud, J.-M.: Infrared nitrogen dioxide: line parameters in the HITRAN database, J. Quant. Spectrosc. Ra., 48, 645–651, 1992.

Randall, C. E., Harvey, V. L., Singleton, C. S., Bernath, P. F., Boone, C. D., and Kozyra, J. U.: Enhanced NO_x in 2006 linked to strong upper stratospheric Arctic vortex, Geophys. Res. Lett., 33, L18811, doi:10.1029/2006GL027160, 2006.

Randall, C. E., Harvey, V. L., Singleton, C. S., Bailey, S. M., Bernath, P. F., Cordrescu, M., Nakajima, H., and Russell III, J. M.: Energetic particle precipitation effects on the Southern Hemisphere stratosphere in 1992–2005, J. Geophys. Res., 112, D08308, doi:10.1029/2006JD007696, 2007.

Randall, C. E., Harvey, V. L., Siskind, D. E., France, J., Bernath, P. F., Boone, C. D., and Walker, K. A.: NO_x descent in the Arctic middle atmosphere in early 2009, Geophys. Res. Lett., 36, L18811, doi:10.1029/2009GL039706, 2009.

Remsberg, E. E. and Bhatt, P. P.: Zonal variances of nitric acid vapor as an indicator of meridional mixing in the subtropical lower stratosphere, J. Geophys. Res., 101(D23), 29523–29530, 1996.

Remsberg, E. E. and Russell III, J. M.: The near global distributions of middle atmospheric H_2O and NO_2 measured by the Nimbus 7 LIMS experiment, in: Transport Processes in the Middle Atmosphere, edited by: Visconti, G. and Garcia, R., D. Reidel Publ. Co., Dordrecht, Holland, 87–102, 1987.

Remsberg, E. E., Natarajan, M., Lingenfelser, G. S., Thompson, R. E., Marshall, B. T., and Gordley, L. L.: On the quality of the Nimbus 7 LIMS Version 6 water vapor profiles and distributions, Atmos. Chem. Phys., 9, 9155–9167, 2009, http://www.atmos-chem-phys.net/9/9155/2009/.

Remsberg, E., Lingenfelser, G., Natarajan, M., Gordley, L., Marshall, B. T., and Thompson, E.: On the quality of the Nimbus 7 LIMS version 6 ozone for studies of the middle atmosphere, J. Quant. Spectrosc. Ra., 105, 492–518, doi:10.1016/j.jqsrt.2006.12.005, 2007.

Remsberg, E. E., Gordley, L. L., Marshall, B. T., Thompson, R. E., Burton, J., Bhatt, P., Harvey, V. L., Lingenfelser, G. S., and Natarajan, M.: The Nimbus 7 LIMS Version 6 radiance conditioning and temperature retrieval methods and results, J. Quant. Spectrosc. Ra., 86, 395–424, doi:10.1016/j.jqsrt.2003.12.007, 2004.

Remsberg, E. E., Bhatt, P. P., Eckman, R. S., Gordley, L. L., Russell III, J. M., and Siskind, D. E.: Effect of the HITRAN 92 spectral data on the retrieval of NO_2 mixing ratios from Nimbus 7 LIMS, J. Geophys. Res., 99, 22965–22973, 1994.

Rothman, L. S., Gamache, R. R., Tipping, R. H., Rinsland, C. P., Smith, M. A. H., Benner, D. C., Devi, V. M., Flaud, J.-M., Camy-Peyret, C., Perrin, A., Goldman, A., Massie, S. T., Brown, L. R., and Toth, R. A.: The HITRAN molecular database: editions of 1991 and 1992, J. Quant. Spectrosc. Ra., 48, 469–507, 1992a.

Rothman, L. S., Hawkins, R. S., Wattson, R. B., and Gamache, R. R.: Energy levels, intensities, and linewidths of atmospheric carbon dioxide bands, J. Quant. Spectrosc. Ra., 48, 537–566, 1992b.

Rothman, L. S., Goldman, A., Gillis, J. R., Tipping, R. H., Brown, L. R., Margolis, J. S., Maki, A. G., and Young, L. D. G.: AFGL trace gas compilation: 1980 edition, Appl. Optics, 20, 1323–1328, 1981.

Russell III, J. M. and Gille, J. C.: The limb infrared monitor of the stratosphere (LIMS) experiment, in The NIMBUS 7 Users' Guide, edited by: Madrid, C. R., NASA Goddard Space Flight Center, Greenbelt, MD., 71–103, 1978.

Russell III, J. R., Gille, J. C., Remsberg, E. E., Gordley, L. L., Bailey, P. L., Drayson, S. R., Fischer, H., Girard, A., Harries, J. E., and Evans, W. F. J.: Validation of nitrogen dioxide results measured by the limb infrared monitor of the stratosphere (LIMS) experiment on NIMBUS 7, J. Geophys. Res., 89, 5099–5107, 1984a.

Russell III, J. M., Solomon, S., Gordley, L. L., Remsberg, E. E., and Callis, L. B.: The variability of stratospheric and mesospheric NO_2 in the polar winter night observed by LIMS, J. Geophys. Res., 89, 7267–7275, 1984b.

Sander, S. P., Friedl, R. R., Ravishankara, A. R., Golden, D. M., Kolb, C. E., Kurylo, M. J., Molina, M. J., Moortgat, G. K., Keller-Rudek, H., Finlayson-Pitts, B. J., Wine, P. A., Huie, R. E., and Orkin, V. L.: Chemical kinetics and photochemical data for use in atmospheric studies – Evaluation Number 15, JPL Publication 06-2, Jet Propulsion Laboratory, Pasadena, CA, 2006.

Solomon, S., Russell III, J. M., and Gordley, L. L.: Observations of the diurnal variation of nitrogen dioxide in the stratosphere, J. Geophys. Res., 91, 5455–5464, 1986.

Thibault, F., Menoux, V., LeDoucen, R., Rosenmann, L., Hartmann, J.-M., and Boulet, C.: Infrared collision-induced absorption by O_2 near 6.4 µm for atmospheric applications: measurements and empirical modeling, Appl. Optics, 36, 563–567, 1997.

Toth, R. A.: High-resolution measurements and analysis of $^{14}N^{16}O_2$ in the [001]-[000] and [011]-[010] bands, J. Opt. Soc. Am. B, 9, 433–461, 1992.

Table 1. Estimates of precision and accuracy (%) for profiles of LIMS V6 HNO_3.

Pressure (hPa)	80	50	30	10	3
Random (PRECISION)	21	4	3	3	10
Calibration	1	1	2	1	7
Temperature Bias	5	1	3	1	6
HNO_3 Spectral Parameters	5	5	5	5	5
CFC & Aerosol Corrections	5	5	2	1	1
Registration & Forward Model Errors	13	6	5	5	5
Root-Sum-Squares (RSS) of bias errors (ACCURACY)	16	9	8	7	12
Unverified Sources of Error					
FOV Side Lobes	27	28	25	27	45
Out-of-band Spectral Signal	29	29	20	7	45

ACPD
10, 2769–2808, 2010

Table 2. Estimates of precision and accuracy (%) for profiles of LIMS V6 NO_2.

Pressure (hPa)	50	30	10	5	3	1
Noise and offset error	5	5	3	3	3	14
H_2O interference	3	3	3	3	5	–
Random (Root-Sum-Squares or RSS Value-PRECISION)	6	6	4	4	6	14
Radiometric Bias Errors	6	6	6	6	6	6
Temperature Bias	22	13	8	8	6	10
H_2O Mixing Ratio	30	13	6	6	8	28
O_2 Cross Section (10%)	34	18	3	1	0	0
NO_2 Line Parameters (10%)	10	10	10	10	10	10
Algorithm/Registration	13	6	5	5	5	5
Main FOV Lobe	5	5	5	5	5	5
RSS of Bias Errors (ACCURACY)	53	29	18	18	17	33
Unverified Source of Error						
FOV Side Lobe Area	1	2	4	1	2	1

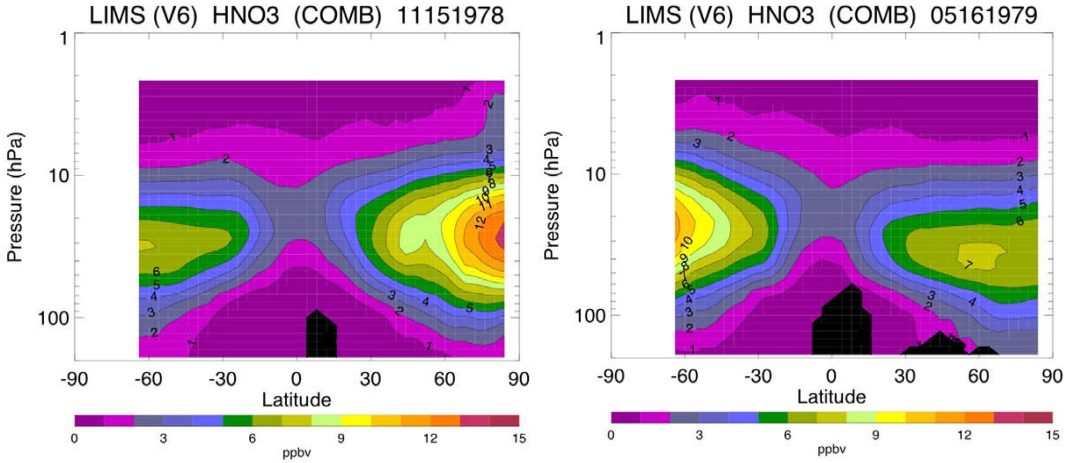

Fig. 1. **(a)** V6 HNO_3 distribution for 15 November 1978, based on the combination (COMB) of the profile data from its ascending and descending orbital segments; blackened regions indicate no data. **(b)** As in (a), but for V6 HNO_3 of 16 May 1979

ACPD
10, 2769–2808, 2010

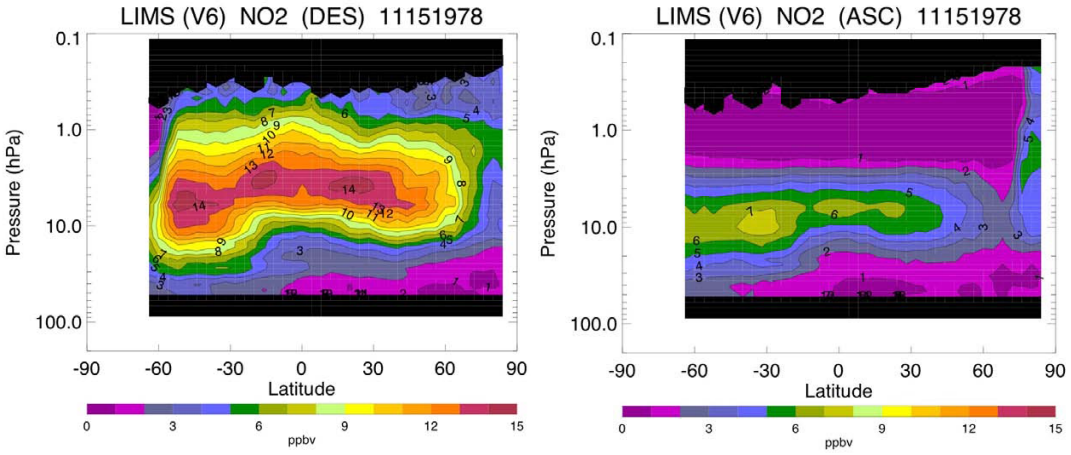

Fig. 2. (a) LIMS V6 distribution of descending (DES or nighttime) NO_2 for 15 November 1978; blackened regions indicate no data. **(b)** As in (a), but for ascending (ASC or daytime) NO_2.

ACPD
10, 2769–2808, 2010

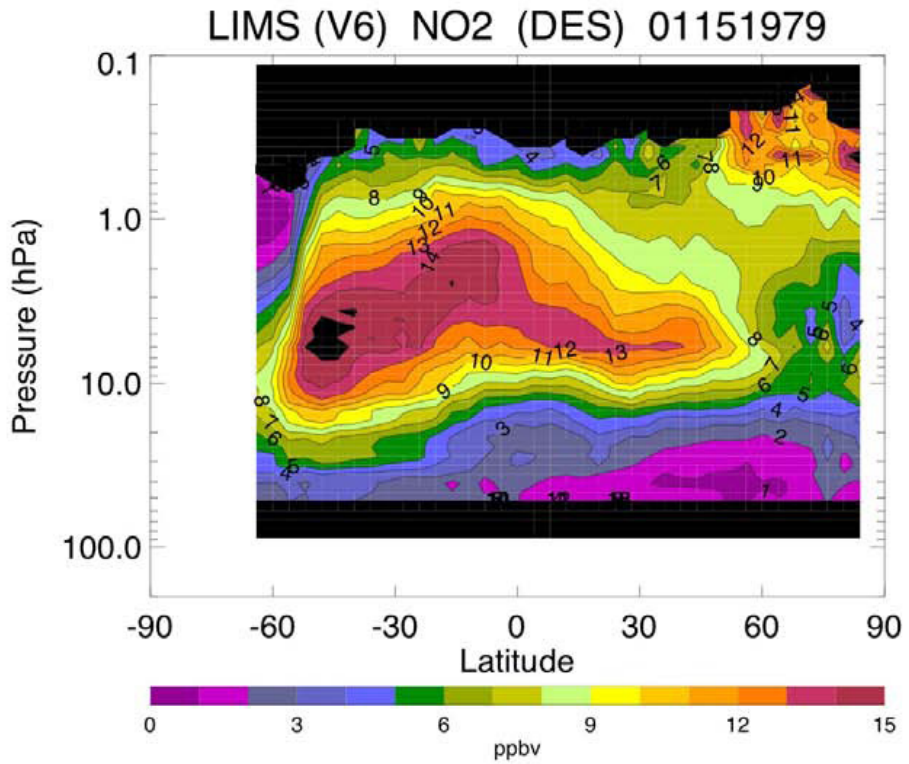

Fig. 3. As in Fig. 2a, but for descending (DES or nighttime) NO_2 of 15 January 1979; blackened region near 50° S, 5 hPa has NO_2 exceeding 15 ppbv.

ACPD
10, 2769–2808, 2010

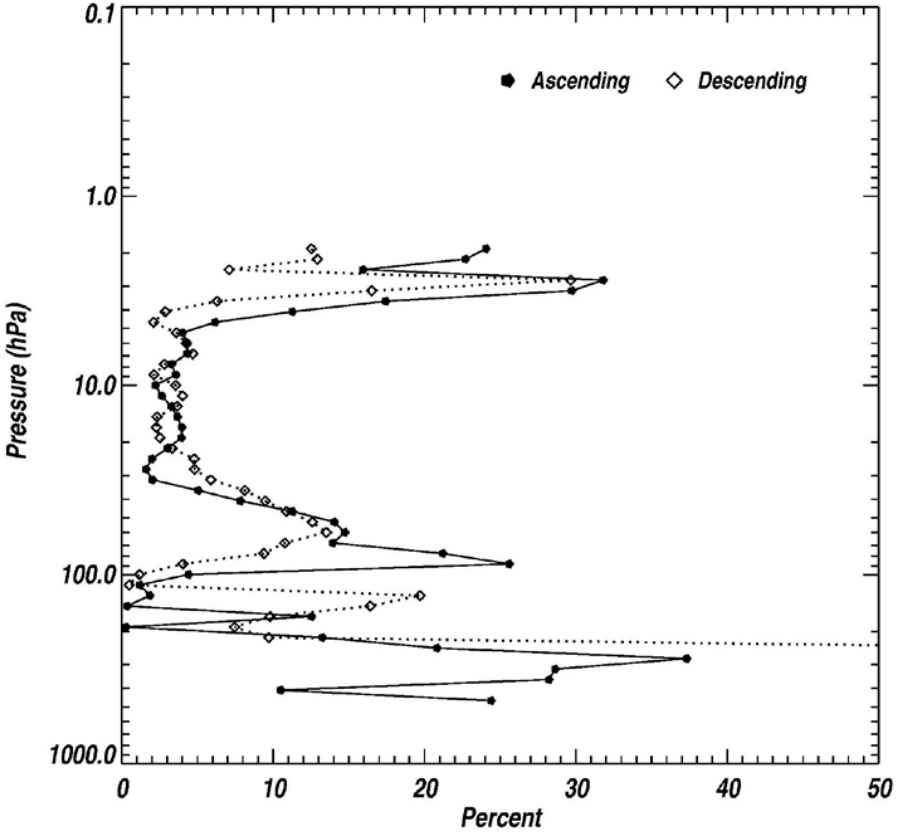

Fig. 4. Estimates of precision based on the minimum standard deviations (SD) of the retrieved LIMS V6 HNO_3 profiles from the sets of ascending (solid) or descending (dashed) orbital crossings of the latitude band of 25° S and 35° S on 1 February 1979.

ACPD
10, 2769–2808, 2010

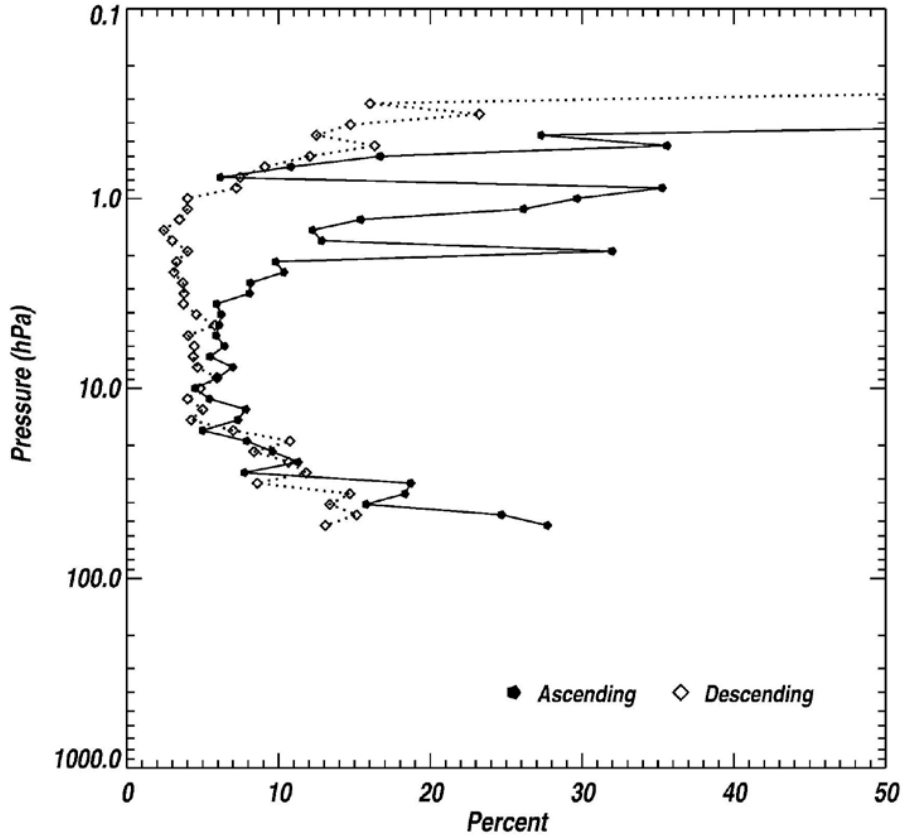

Fig. 5. As in Fig. 4, but for estimates of precision (SD) for LIMS V6 NO_2 profiles.

ACPD
10, 2769–2808, 2010

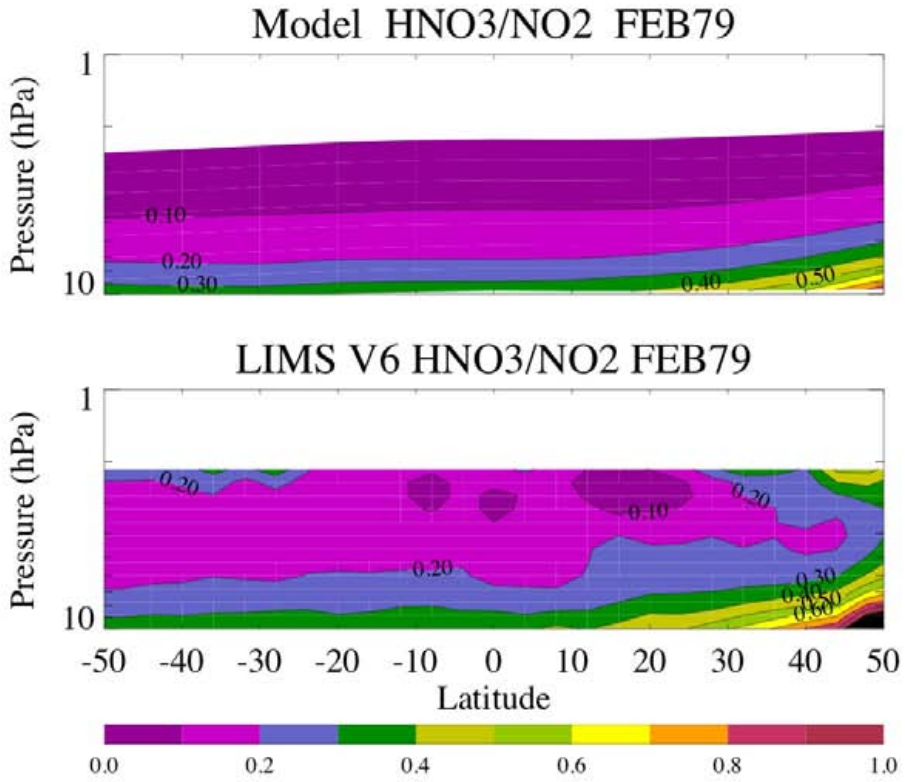

Fig. 6. HNO_3/NO_2 ratios for February 1979 – (top) model and (bottom) LIMS V6 data.

ACPD
10, 2769–2808, 2010

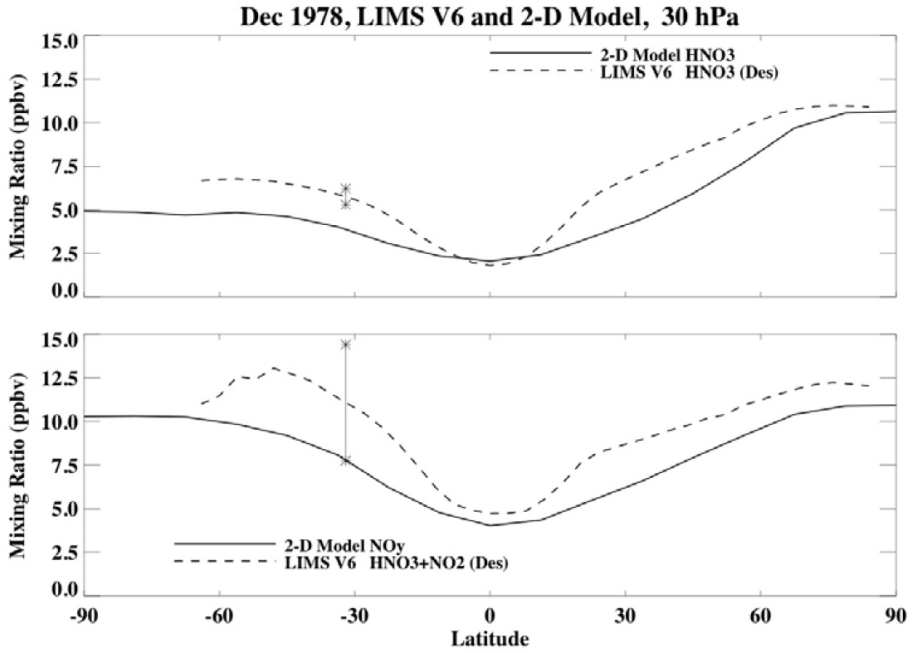

Fig. 7. LIMS V6 (dashed) and model (solid) comparisons for December 1978 – (top) HNO_3 and (bottom) HNO_3+NO_2 for the LIMS descending (DES or nighttime) orbital segments. The vertical lines on the LIMS data at 32° S denote their associated uncertainties.

ACPD
10, 2769–2808, 2010

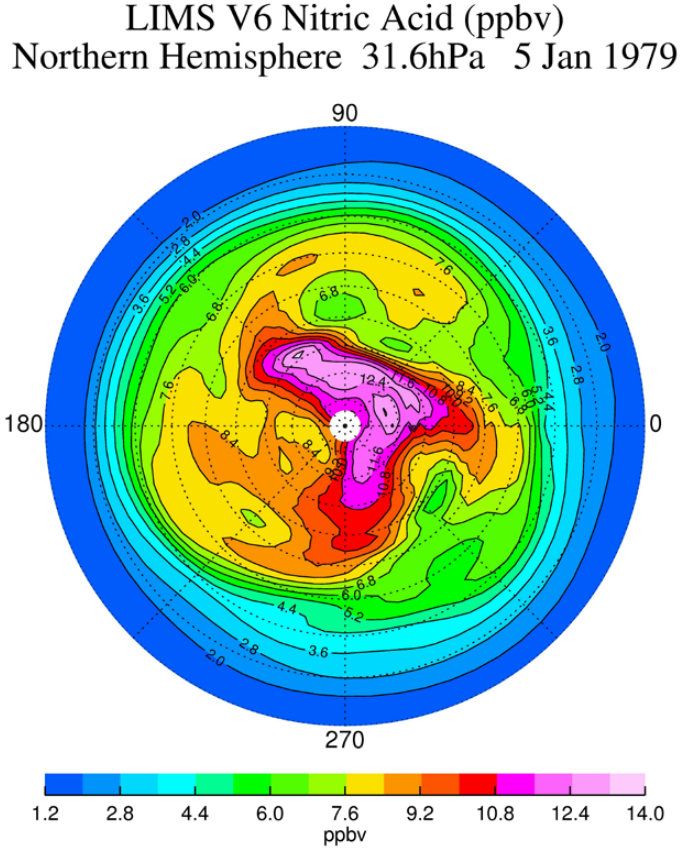

Fig. 8. Polar plot of ascending plus descending V6 HNO_3 for 5 January 1979. Bluish regions are low values and orange to pink regions are high values; contour interval is 0.8 ppbv.

ACPD
10, 2769–2808, 2010

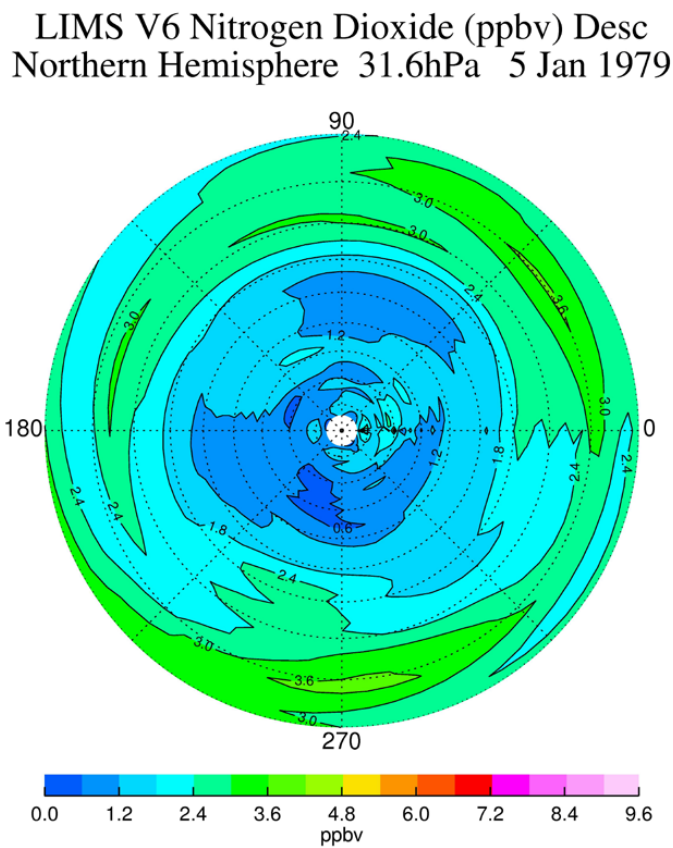

Fig. 9. Polar plot of V6 descending NO_2 for 5 January 1979. Bluish regions are low values and greenish regions are high values; contour interval is 0.6 ppbv.

ACPD
10, 2769–2808, 2010

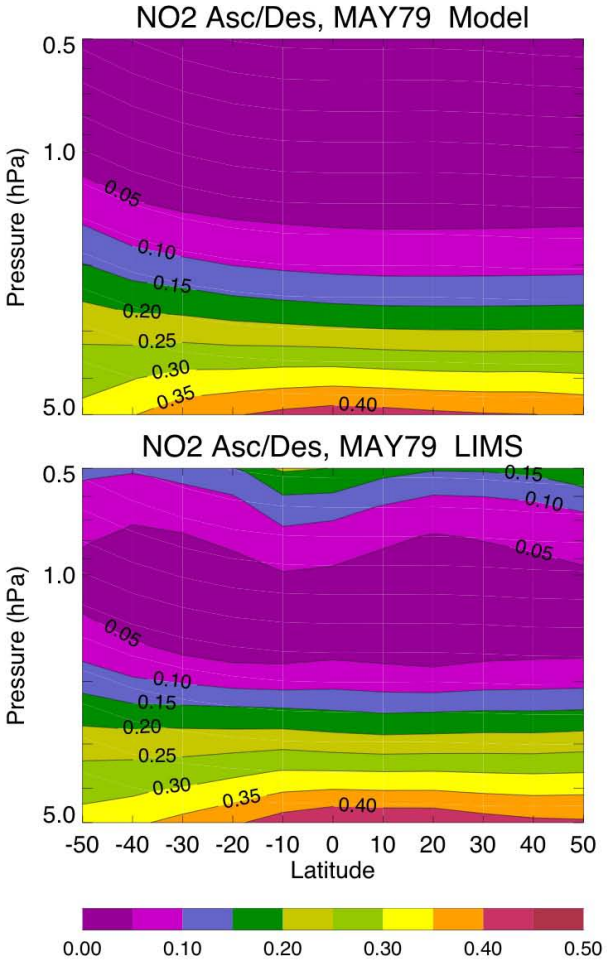

Fig. 10. Ascending/descending (or day/night) NO_2 ratio (top) diurnal model and (bottom) LIMS V6.

ACPD
10, 2769–2808, 2010

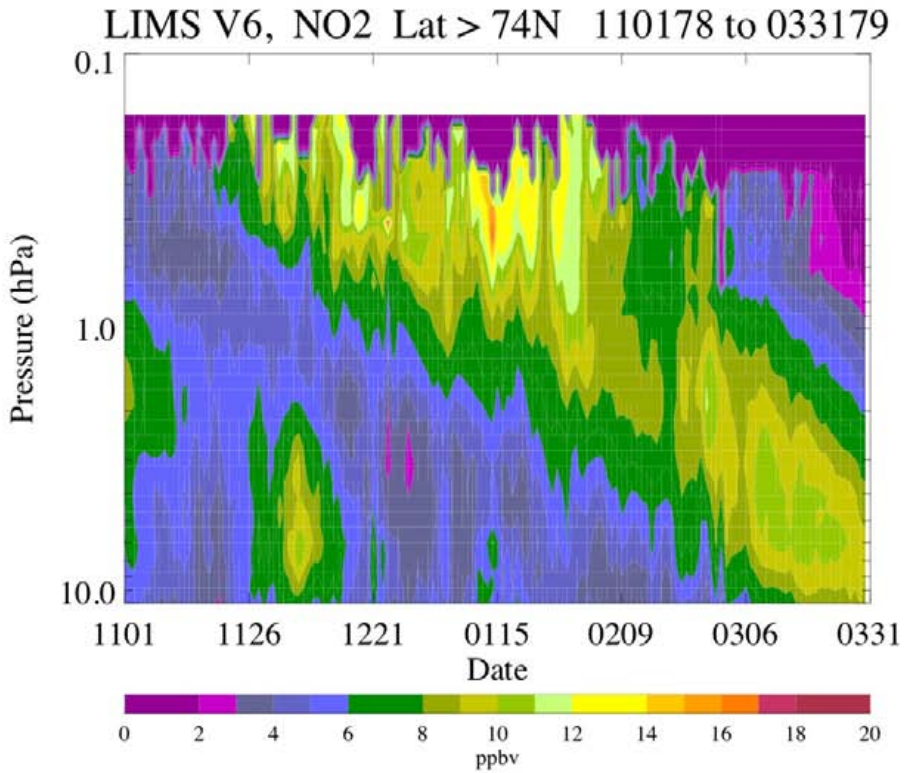

Fig. 11. Time series of LIMS V6 NO_2 for latitudes >74° N. For those few days when no data were taken, the NO_2 values are averages from the adjacent days.

ACPD
10, 2769–2808, 2010